Influence of free-carrier absorption on terahertz generation from ZnTe(110)

Shayne M. Harrel,[a] Rebecca L. Milot, James M. Schleicher,[b] and Charles A. Schmuttenmaer[c]
Department of Chemistry, Yale University, 225 Prospect Street, New Haven, Connecticut 06520-8107, USA

(Received 6 October 2009; accepted 21 December 2009; published online 11 February 2010)

ZnTe(110) is widely used as a source of terahertz radiation generated by optical rectification. However, when ZnTe(110) is excited with 800 nm light, optical rectification is not the only process which can occur. Specifically, second harmonic generation and two-photon absorption are also possibilities. In addition, free carriers generated by two-photon absorption can absorb terahertz radiation, further reducing the efficiency of optical rectification. We have used terahertz emission spectroscopy to study these effects by analyzing the dependence of the terahertz waveform on excitation fluence. At high excitation fluences, the overall efficiency is reduced and the trailing edge of the waveform is attenuated. A simple model reproduces the measured behavior.
 [doi:10.1063/1.3296064]

I. INTRODUCTION

Early experiments on ZnTe(110) showed that it was the material of choice as a bright, broadband source of terahertz radiation from tabletop Ti:Sapphire lasers via optical rectification.[1–5] ZnTe has a large second-order nonlinear susceptibility, it is nearly transparent in the terahertz region of the spectrum, and it has favorable phase-matching conditions with ~800 nm light that allow it to produce large-amplitude, broad-bandwidth pulses in the far-infrared. As the interest in studying phenomena in the far-infrared region of the spectrum grows, so does the demand for bright sources of terahertz radiation.[6] Thus, maximizing the efficiency of terahertz emission from ZnTe(110) has received much attention. For example, Xu and Zhang[7] conducted studies of optical rectification in ZnTe(110) as a function of the optical excitation area when exciting an area smaller than the central terahertz emission wavelength. More recently, studies have shown that processes such as second harmonic generation (SHG), two-photon absorption (TPA), and free-carrier absorption (FCA) can all compete with optical rectification.[8–12]

SHG is the sum-frequency analog of optical rectification and removes photons from the excitation pulse that would normally produce terahertz radiation. TPA also depletes the excitation beam intended for optical rectification and more importantly, produces free carriers, which can then absorb the generated terahertz radiation through FCA. These processes reduce the efficiency of terahertz generation in ZnTe(110) and become problematic at high excitation intensities. Although many papers which analyze these processes have been published, the available literature is often incomplete and contradictory. For example, Gaivoronskii *et al.*[9] conclude that TPA and FCA are not responsible for attenuating terahertz radiation at high powers, whereas Zhao and Tignon[11] identify a strong contribution from FCA of terahertz radiation. Others admit that TPA decreases the excitation power available for terahertz generation but do not analyze the effects of FCA after terahertz generation.[10]

In many of these studies, the *z*-scan method is employed to vary excitation fluence. One concern when monitoring terahertz emission is that the small beam diameters used will lead to significant diffraction of the terahertz pulse.[7,10] In the present study, excitation fluence is varied independently of laser spot size in order to focus solely on the effects of TPA and FCA on terahertz generation. Additionally, optical rectification in ZnTe(110) has not been investigated in regions of lesser excitation powers since the goal has always been to produce the largest amplitude terahertz pulses possible, and little to no attention has been paid to the shape of the generated waveforms over the range of intensities. Using terahertz emission spectroscopy, this study analyzes the shapes of the generated waveforms and relates them to trends in terahertz amplitude over a wide range of excitation fluences.

II. EXPERIMENTAL

The experimental apparatus has been detailed elsewhere.[13] In brief, a regeneratively amplified Ti:Sapphire laser produces ~100 fs pulses centered at 800 nm at a repetition rate of 1 kHz. The output beam is split into two parts: terahertz generation and detection. The 8.8 mm diameter generation beam photoexcites the 1.0 mm thick ZnTe(110) sample, and the detection beam detects the emitted terahertz radiation in a second 1.0 mm thick ZnTe(110) crystal via free space electro-optic sampling (FSEOS).[14–16] The ZnTe sample is positioned 4 cm from the ZnTe detector to analyze the terahertz waveform in the far-field. A half-wave plate and a quartz polarizer placed before the sample serve as a variable attenuator and control the fluence of the excitation beam. A silver nanorod polarizer between the quartz polarizer and the sample ensures that the polarization is as clean as possible. See Fig. 1(a) for a schematic diagram.

Excitation powers above 10 mW (the corresponding fluence is 17 $\mu J/cm^2$) are measured using a power meter

[a]Present address: Food & Drug Administration, Winchester Analytical and Engineering Center, 109 Holton St., Winchester, Massachusetts 01890, USA.
[b]Present address: The University of Michigan Law School, 625 South State Street, Ann Arbor, Michigan, 48109-1215, USA.
[c]Electronic mail: charles.schmuttenmaer@yale.edu.

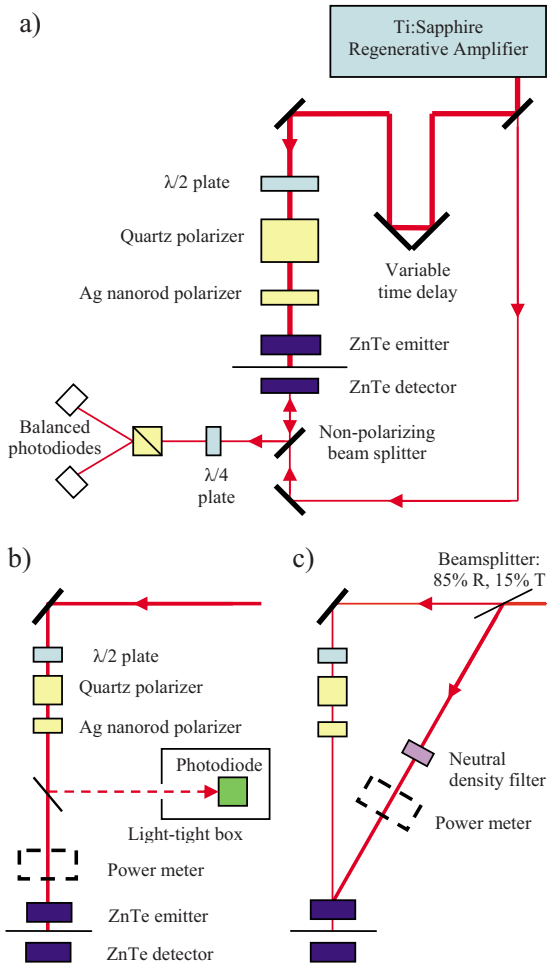

FIG. 1. (Color online) Part (a) diagrams the basic terahertz emission setup, part (b) shows the modifications for low fluence measurements, and part (c) includes optics for the fixed time-delay pump-probe configuration.

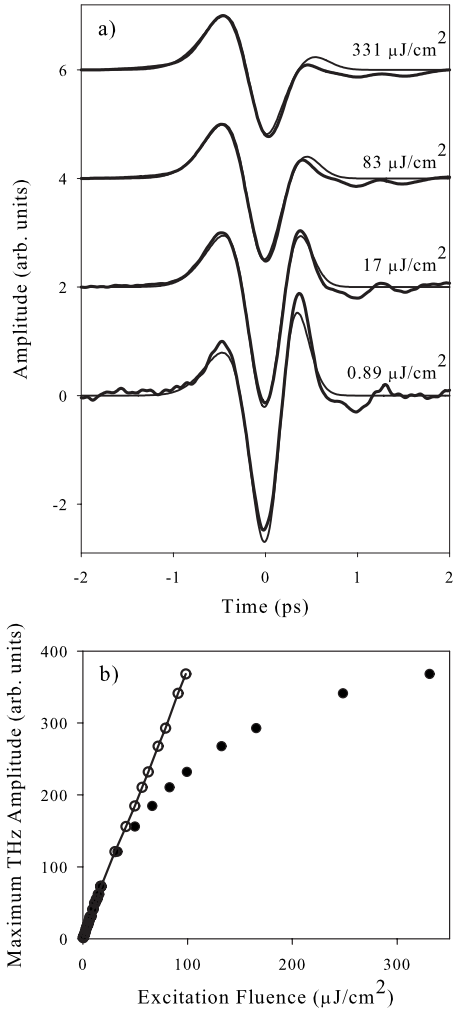

FIG. 2. In part (a), terahertz waveforms obtained over the range of excitation fluences are displayed. The thicker lines are the experimental data, and the thinner lines are fits of Eq. (4) to the experimental data. The waveforms have been scaled and offset vertically to clearly demonstrate the changes in shape. Part (b) shows the dependence of terahertz amplitude on excitation fluence. The filled circles represent the raw experimental data, and the open circles have been corrected for pump depletion due to TPA.

(Spectra Physics, Model 407A). For powers below 10 mW, a Si photodiode is used; a microscope slide is placed before the sample, and a small portion of the excitation beam is directed at the Si photodiode as seen in Fig. 1(b). It is important to place the photodiode inside a light-tight enclosure to ensure that stray reflections do not contribute to the measured power. If necessary, filters are used to ensure that the photodiode is not saturated. The photodiode response is calibrated to a power measurement using the power meter at an excitation power of 10 mW.

The basic terahertz emission setup can be transformed to examine the effects of photoexcitation of the emitter prior to terahertz generation. As seen in Fig. 1(c), a pump pulse at fixed delay time is introduced. Specifically, a beam splitter that transmits 15% and reflects 85% of the power is placed before the final turning mirror to create a pump beam (85%) which photoexcites the sample and a secondary beam for terahertz generation in the photoexcited sample. The secondary beam fluence is 66 $\mu J/cm^2$, and the pump fluence ranges from 0 to 281 $\mu J/cm^2$. Neutral density filters are placed in the pump beam path to vary the photoexcitation fluence. The geometry of this setup ensures that the pump pulse always arrives 265 ± 10 ps before the terahertz generation pulse and that only terahertz radiation created from the secondary beam is detected.

III. RESULTS AND DISCUSSION

A series of terahertz waveforms were collected at excitation fluences ranging from 0.58–331 $\mu J/cm^2$. Figure 2 shows representative scaled waveforms obtained at high, low, and mid-range fluences in part (a) as well as a plot of the dependence of terahertz amplitude on excitation fluence in part (b). At excitation fluences below 17 $\mu J/cm^2$, the time-dependence of the terahertz waveform resembles the second derivative of the Gaussian excitation pulse, which is the shape expected for optical rectification with detection in the far field.[17–19] At higher fluences, however, the waveform is noticeably attenuated at later times and more closely resembles the first derivative of the Gaussian excitation pulse. The filled circles in part (b) show that the terahertz amplitude varies linearly with excitation fluences below 17 $\mu J/cm^2$ as expected for optical rectification but is sublinear above 33 $\mu J/cm^2$. Since optical rectification is a second-order nonlinear process, the terahertz intensity should vary quadrati-

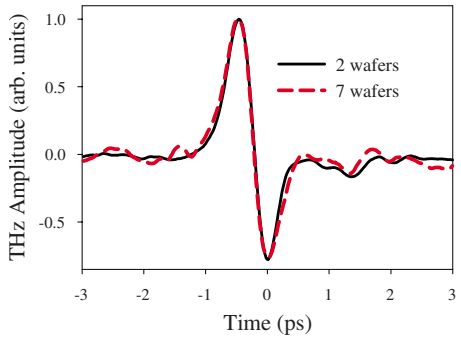

FIG. 3. (Color online) Result of attenuating terahertz pulse with two and seven Si wafers to demonstrate that the difference in waveforms at high and low power cannot be attributed to the detector. The waveforms have been scaled in order to compare their shapes.

cally with input power. This is equivalent to stating that the terahertz amplitude should vary linearly with input power.

Three distinct possibilities for the unexpected dependence of terahertz amplitude on excitation fluence have been examined: 1. a nonlinear detector response, 2. the terahertz generation mechanism itself (shift currents vs. optical rectification), and 3. optical rectification coupled with FCA of terahertz radiation due to TPA of the excitation pulse. We conclude that the third is operative.

A. Detector response

It is conceivable that the ZnTe(110) detector responds nonlinearly as a function of incident terahertz amplitude. To test whether the waveform is altered due to a nonlinear response of the detector, the ZnTe(110) emitter was excited at 230 $\mu J/cm^2$, and the terahertz pulse generated was attenuated using a set of high-resistivity Si wafers. The Si wafers have an index of refraction of 3.4, which is independent of frequency in the terahertz region.[20] Thus, each wafer attenuates the terahertz amplitude by ~55% but does not distort the waveform. The results of placing two and seven Si wafers in the terahertz beam path are shown in Fig. 3 with the waveforms scaled for comparison. Attenuating the terahertz amplitude does not change the shape of the detected pulse. Additionally, when seven wafers are used, the measured terahertz amplitude is on the same order of magnitude as what is obtained when exciting the emitter at the lower fluences of $\sim 2.5\ \mu J/cm^2$. This result proves that the dependence of the measured terahertz waveform as a function of excitation fluence is not affected by the detector.

B. Mechanism of terahertz generation

Optical rectification is not the only mechanism through which terahertz radiation can be generated. From the theoretical work of Sipe,[18,21] it is known that there are two contributions to the time-dependent current densities in zincblende semiconductors that can lead to terahertz emission. For above bandgap excitation, shift currents dominate, while optical rectification is the primary mechanism when exciting below the bandgap. When detecting in the far-field,[17] terahertz radiation due to shift currents has a waveform that follows the first time-derivative of the time-varying excitation pulse intensity, while rectification currents produce terahertz radiation having a waveform that is the second time derivative. Experiments carried out by Cote *et al.*[22] and more recently by Schleicher *et al.*[19] have experimentally verified this time-derivative relationship between terahertz radiation generated by shift currents and optical rectification in GaAs.

The bandgap of ZnTe is 2.3 eV at 300 K.[23] Therefore, a shift current in ZnTe excited at 800 nm (photon energy of 1.55 eV) would have to be the result of a two-photon process. Although the shape of the waveforms obtained at high fluences are consistent with terahertz generation through a shift current, the positions of the maxima, minima, and zero crossings of the terahertz waveforms as a function of excitation fluence confirm that optical rectification is the only mechanism responsible. In particular, the first derivative of a Gaussian crosses zero when the second derivative reaches its minimum. Therefore, if the mechanism of terahertz generation were changing from optical rectification to shift current, then the peaks and zero crossings of the waveforms would shift relative to each other. Looking at Fig. 2, these features occur at the same delay time when exciting with different fluences; only their relative amplitudes change. Therefore, all of the waveforms result from the same underlying generation mechanism: optical rectification.

C. FCA and TPA

TPA of the excitation beam and FCA of terahertz radiation have been identified as processes that compete with optical rectification.[8–12] We find that FCA attenuates the latter part of the terahertz pulse, while TPA depletes the power available for terahertz generation.

1. FCA

We have developed a simple model to explain the influence of FCA on the *shape* of the generated terahertz waveform as a function of excitation fluence. While the general result of attenuation due to FCA is consistent with previous workers' results,[11] no one has previously demonstrated its influence as a function of time as the pulse is being generated. Previous studies measured the terahertz power using a bolometer, which is not time-resolved on the timescale of the terahertz waveform and which measures intensity rather than the terahertz amplitude as done using FSEOS.

The terahertz waveforms obtained at different excitation fluences were modeled by including the effects of FCA *during* the generation process. That is, the excitation pulse simultaneously generates a terahertz pulse through optical rectification as well as creating free carriers via TPA, which then attenuate the latter part of the pulse. A slightly skewed Gaussian intensity profile of the optical excitation beam (I_{opt}) is assumed. This was required because at the lowest excitation powers, where FCA does not play a role, the second positive lobe of the terahertz waveform is larger than the first [see Fig. 2(a)].

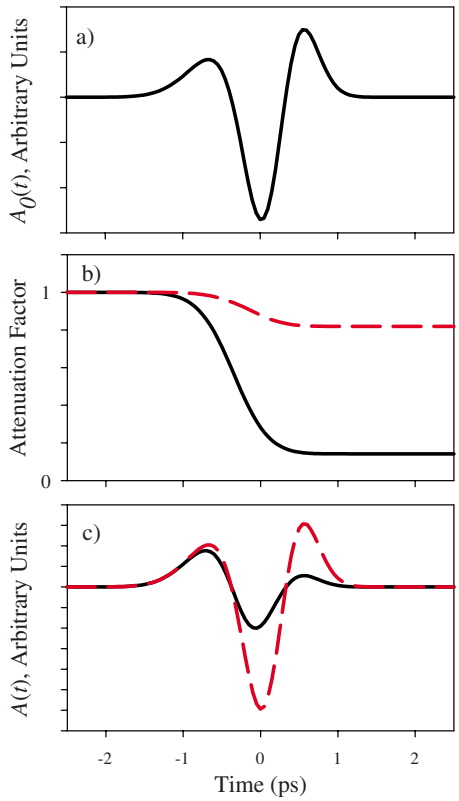

FIG. 4. (Color online) Part (a) shows the expected terahertz pulse shape in the absence of TPA or FCA calculated using Eq. (1). This is essentially what is measured at the lowest excitation fluences. Part (b) is attenuation as a function of time at high (solid) and low (dashed) fluences, and part (c) is the product of parts (a) and (b).

$$I_{\mathrm{opt}}(t) = \exp\left[-\left(\frac{t-t_0}{2\sigma}\right)^2\right]\frac{1}{2}\left[1+\mathrm{erf}\left(\alpha\frac{t-t_0}{\sqrt{2}\sigma}\right)\right], \tag{1}$$

where t_0 is the center of the Gaussian, σ is its standard deviation (which is related to the full width at half maximum by $w_{\mathrm{FWHM}}=4\sigma\sqrt{\ln 2}$), α is the "skew parameter," and "erf" is the error function. In the absence of FCA, the amplitude of the terahertz waveform is given by the second derivative of the input intensity

$$A_0(t) = \frac{d^2 I_{\mathrm{opt}}(t)}{dt^2}. \tag{2}$$

Figure 4(a) shows $A_0(t)$.

Electrons are generated by TPA, and thus the electron density as a function of time is given by the integral of the square of the excitation pulse (since electron generation is a two-photon process)

$$N_{\mathrm{e}}(t) = \frac{\int_{-\infty}^{t} I_{opt}^2(t')dt'}{\int_{-\infty}^{\infty} I_{opt}^2(t')dt'}. \tag{3}$$

The integral in the denominator ensures that the value at long times is 1.

Figure 4(b) shows the amount of attenuation as a function of time during the excitation pulse for high power and low power excitation (solid and dashed lines, respectively). The functional form of the attenuation is $\exp[-N_{\mathrm{e}}(t)e_{\mathrm{scale}}]$, where $N_{\mathrm{e}}(t)$ is the electron density, and e_{scale} is a scaling factor that is adjusted to give the best agreement between the calculated and measured waveforms. Finally, the terahertz waveforms, $A(t)$, which are compared to the experimental ones are the products of $A_0(t)$ and the amount of attenuation. Specifically

$$A(t) = aA_0(t)e^{-N_{\mathrm{e}}(t)e_{\mathrm{scale}}}, \tag{4}$$

where a is a scaling factor that is adjusted to obtain the best fit with experiment. Figure 4(c) displays $A(t)$ for the attenuation factors given in part (b).

Equation (4) was fit to the experimental data using the Marquardt–Levenberg nonlinear least-squares fitting algorithm. As seen in Fig. 2(a), this model reproduces all of the important features of the waveforms over the full range of excitation fluences. The fitting parameters are given in Table I, and the results for all 24 waveforms collected in this study can be found in the supplementary information.[24]

2. TPA

In order to verify that TPA generates carriers which lead to FCA, the excitation beam was split such that the sample was photoexcited 265 ± 10 ps before terahertz generation [see Fig. 1(c)]. The photoexcitation or "pump" fluence was varied from 0 to 281 $\mu\mathrm{J/cm^2}$ while the terahertz generation fluence was held constant at 66 $\mu\mathrm{J/cm^2}$. The results of this pump-probe experiment are shown in Fig. 5(a). At all excitation fluences, the entire terahertz waveform is attenuated because the pump arrives well before the optical pulse that generates the terahertz waveform.

When a material undergoes TPA, the intensity I at a distance l within a sample illuminated with incident intensity I_0 is given by $I=I_0/(1+I_0\beta l)$, where β is the TPA coefficient ($\beta=4.6$ cm/GW for ZnTe(110) and 800 nm light).[11,12,25] Fig. 5(b) plots the relative terahertz amplitude as a function of pump fluence, and it is seen that the attenuation of the terahertz pulse is accounted for quantitatively by considering the TPA of the pump pulse. The line is obtained using values of $I_0=3.2$ GW/cm^2, $\beta=4.6$ cm/GW, and $l=0.1$ cm. The

TABLE I. Best fit parameters for waveforms shown in Fig. 2(a). Uncertainties in parentheses are 1σ.

Fluence ($\mu\mathrm{J/cm^2}$)	t_0 (ps)	FWHM (ps)	Amplitude	e_{scale}	α
0.89	0.145(1.5)	0.796(5.2)	2.46(6.0)	1.00×10^{-5}[a]	−1.59[a]
17	0.189(1.4)	0.807(3.5)	68.0(8.8)	0.85(2.3)	−1.59[a]
83	0.270(2.2)	0.880(4.5)	274(3.2)	1.61(2.7)	−1.59[a]
331	0.343(3.9)	0.957(7.4)	593(8.6)	2.14(4.1)	−1.59[a]

[a]These values were held fixed during the fit.

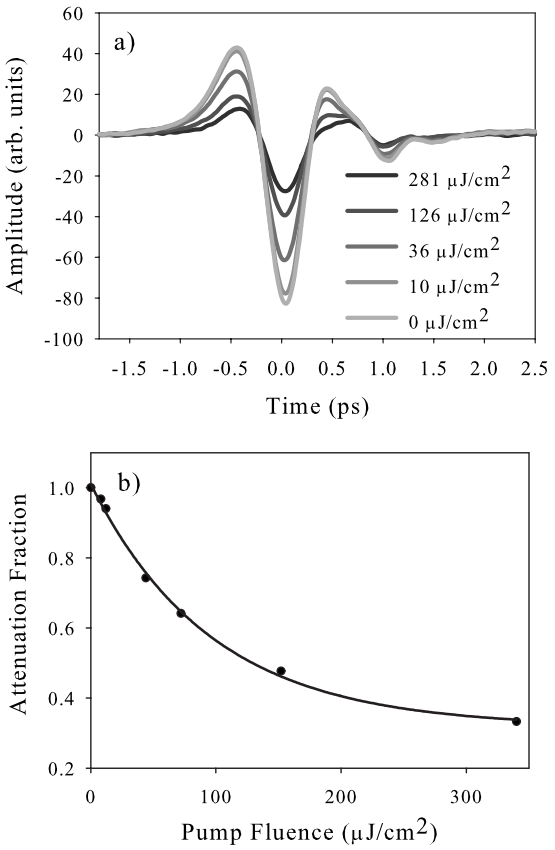

FIG. 5. Part (a) shows the attenuation of the terahertz waveform with increasing pump fluence for the pump/probe experiment. In part (b), the transmitted fraction of the terahertz amplitude is shown as a function of pump fluence.

value of I_0 that gives the best fit is slightly higher than the actual value of 2.8 GW/cm^2 because of multiple internal reflections within the ZnTe wafer.

Looking back to Fig. 2(b), the sublinear dependence of terahertz amplitude on excitation fluence is explained by pump depletion due to TPA. Specifically, the open circles in Fig. 2(b) are plotted as a function of available fluence (or TPA-depleted fluence) rather than incident fluence, and the resulting dependence is linear.

IV. CONCLUSION

The amplitude dependence as a function of excitation fluence of terahertz pulses generated from ZnTe(110) with 800 nm light has been investigated using terahertz emission spectroscopy. The divergence from linearity is attributed to a combination of FCA of the generated terahertz radiation as well as TPA leading to depletion of the excitation beam. The possibilities of nonlinearity in the electro-optic response of the detector as well as terahertz generation mechanisms other than optical rectification were discounted as possible causes for the observed fluence dependence. Optical pumping prior to terahertz generation confirmed the influence of both TPA and FCA, and a model was developed that accounts for FCA *during* the excitation pulse.

ACKNOWLEDGMENTS

We acknowledge the National Science Foundation (Grant No. CHE-0616875) for partial support of this work. S.M.H. and R.L.M. contributed equally to this work.

[1]Q. Chen and X. C. Zhang, Appl. Phys. Lett. **74**, 3435 (1999).
[2]A. Nahata, A. S. Weling, and T. F. Heinz, Appl. Phys. Lett. **69**, 2321 (1996).
[3]D. H. Auston, K. P. Cheung, J. A. Valdmanis, and D. A. Kleinman, Phys. Rev. Lett. **53**, 1555 (1984).
[4]T. J. Carrig, G. Rodriguez, T. S. Clement, A. J. Taylor, and K. R. Stewart, Appl. Phys. Lett. **66**, 121 (1995).
[5]L. Xu, X. C. Zhang, and D. H. Auston, Appl. Phys. Lett. **61**, 1784 (1992).
[6]C. A. Schmuttenmaer, Chem. Rev. (Washington, D. C.) **104**, 1759 (2004).
[7]J. Z. Xu and X. C. Zhang, Opt. Lett. **27**, 1067 (2002).
[8]G. L. Dakovski, B. Kubera, and J. Shan, J. Opt. Soc. Am. B **22**, 1667 (2005).
[9]V. Y. Gaivoronsky, M. M. Nazarov, D. A. Sapozhnikov, Y. V. Shepelyavyi, S. A. Shkel'nyuk, A. P. Shkurinov, and A. V. Shuvaev, IEEE J. Quantum Electron. **35**, 407 (2005).
[10]Q. R. Xing, L. Y. Lang, Z. Tian, N. Zhang, S. X. Li, K. Wang, L. Chai, and Q. Wang, Opt. Commun. **267**, 422 (2006).
[11]Z. Y. Zhao and J. Tignon, AIP Conf. Proc. **893**, 503 (2007).
[12]Z. Y. Zhao, S. Hameau, and J. Tignon, Chin. Phys. Lett. **25**, 1868 (2008).
[13]E. Beaurepaire, G. M. Turner, S. M. Harrel, M. C. Beard, and J. Y. Bigot, Appl. Phys. Lett. **84**, 3465 (2004).
[14]M. C. Beard, G. M. Turner, and C. A. Schmuttenmaer, Phys. Rev. B **62**, 15764 (2000).
[15]Z. G. Lu, P. Campbell, and X. C. Zhang, Appl. Phys. Lett. **71**, 593 (1997).
[16]K. Reimann, R. P. Smith, A. M. Weiner, T. Elsaesser, and M. Woerner, Opt. Lett. **28**, 471 (2003).
[17]A. E. Kaplan, J. Opt. Soc. Am. B **15**, 951 (1998).
[18]J. E. Sipe and A. I. Shkrebtii, Phys. Rev. B **61**, 5337 (2000).
[19]J. M. Schleicher, S. M. Harrel, and C. A. Schmuttenmaer, J. Appl. Phys. **105**, 113116 (2009).
[20]S. E. Ralph, S. Perkowitz, N. Katzenellenbogen, and D. Grischkowsky, J. Opt. Soc. Am. B **11**, 2528 (1994).
[21]F. Nastos and J. E. Sipe, Phys. Rev. B **74**, 035201 (2006).
[22]D. Côté, N. Laman, and H. M. van Driel, Appl. Phys. Lett. **80**, 905 (2002).
[23]M. Schall and P. U. Jepsen, Appl. Phys. Lett. **80**, 4771 (2002).
[24]See supplementary material at http://dx.doi.org/10.1063/1.3296064 for additional material pertaining to the nonlinear least-squares fits and the influence of self-phase modulation.
[25]M. Yin, H. P. Li, S. H. Tang, and W. Ji, Appl. Phys. B: Lasers Opt. **70**, 587 (2000).

Supplementary Information for:
Influence of Free-carrier Absorption on Terahertz Generation from ZnTe(110)

Shayne M. Harrel,[†,a] Rebecca L. Milot,[†] James M. Schleicher,[b] Charles A. Schmuttenmaer[c)]
Yale University, Department of Chemistry, 225 Prospect St., New Haven, CT 06520-8107 USA

[†]These authors contributed equally to this work.
[a)]Current address: Food & Drug Administration, Winchester Analytical and Engineering Center, 109 Holton St., Winchester, MA 01890 USA
[b)]Current address: The University of Michigan Law School, 625 South State Street, Ann Arbor, Michigan, 48109-1215 USA
[c)]Electronic mail: charles.schmuttenmaer@yale.edu

December 17, 2009

This document contains additional material pertaining to the nonlinear least squares fits and the influence of self phase modulation.

Results of nonlinear least squares fits

The blue lines in Figure S1 are twenty four waveforms which were collected with excitation fluences ranging from 0.58 μJ/cm^2 (upper left corner) to 331 μJ/cm^2 (lower right corner). The thin red lines are the result of the best fits. The vertical axes have been scaled such that all the THz waveforms are roughly the same height. It is seen that good fits are obtained at all fluence levels.

Figure S2 presents the best fit parameters. The red circles connected by thin red lines are obtained when plotting each parameter as a function of fluence striking the sample. The thick blue lines are the same values for the parameters accounting for the loss of photons due to two-photon absorption; *i.e.*, the TPA-depleted fluence is used instead of the fluence striking the sample. The most important result is that the scale factor in part (c) varies linearly with the TPA-depleted fluence, indicating that the THz emission is due to optical rectification.

It is seen that the Gaussian center and FWHM [parts (a) and (b)] increase as a function of increasing fluence. The delay and broadening are attributed to self-phase modulation (SPM) of the excitation pulse. To verify the effects of SPM, a ZnTe(110) crystal was placed between two variable attenuators prior to the emitter, as shown in Figure S3a. Each variable attenuator consists of a half-wave plate and a polarizer that passes horizontal polarization. At high intensities, the first crystal [ZnTe(110) #1] changes the shape of the optical pulse before it arrives at the emitter [ZnTe(110) #2]. The two traces in Figure S3b were obtained with the same fluence, 17 μJ/cm^2, on the emitter.

The red trace was obtained by rotating the half-wave plate in variable attenuator #2 such that a maximum amount of light was transmitted through it. Then the half-wave plate in variable attenuator #1 was rotated until the fluence at the emitter was 17 μJ/cm^2 and the fluence at ZnTe #1 was 69 μJ/cm^2. The second configuration, which yielded the black trace in Figure S3b, has the half-wave plate in attenuator #1 rotated such that maximum power is transmitted through it and the fluence at ZnTe #1 is 234 μJ/cm^2. Then the half-wave plate in attenuator #2 is rotated such that the fluence at the emitter is 17 μJ/cm^2. There is more TPA in ZnTe(110) #1 in this configuration compared to the first configuration. The optical pulse passes through all the same components in both configurations; the only difference is the amount of power travelling through ZnTe(110) #1. The black trace has been broadened and shifted relative to the red trace, and the peak THz amplitude is smaller because the optical pulse has been broadened. Both effects are indicative of SPM.

The e_{scale} parameter does not vary linearly with fluence, whether or not the incident or TPA-depleted fluence is used. This could be due to multiphoton absorption to lower mobility regions of the band structure or a decreased mobility as a function of electron density. This behavior will be investigated in future work.

The skewness was held fixed at the same values for all of the fits. Initially, it was allowed to vary for all of the fits, but its value always was between –1.4 and –1.8. Therefore, a value of –1.6 was chosen. Letting it vary for each fit did not change the trends in the other parameters.

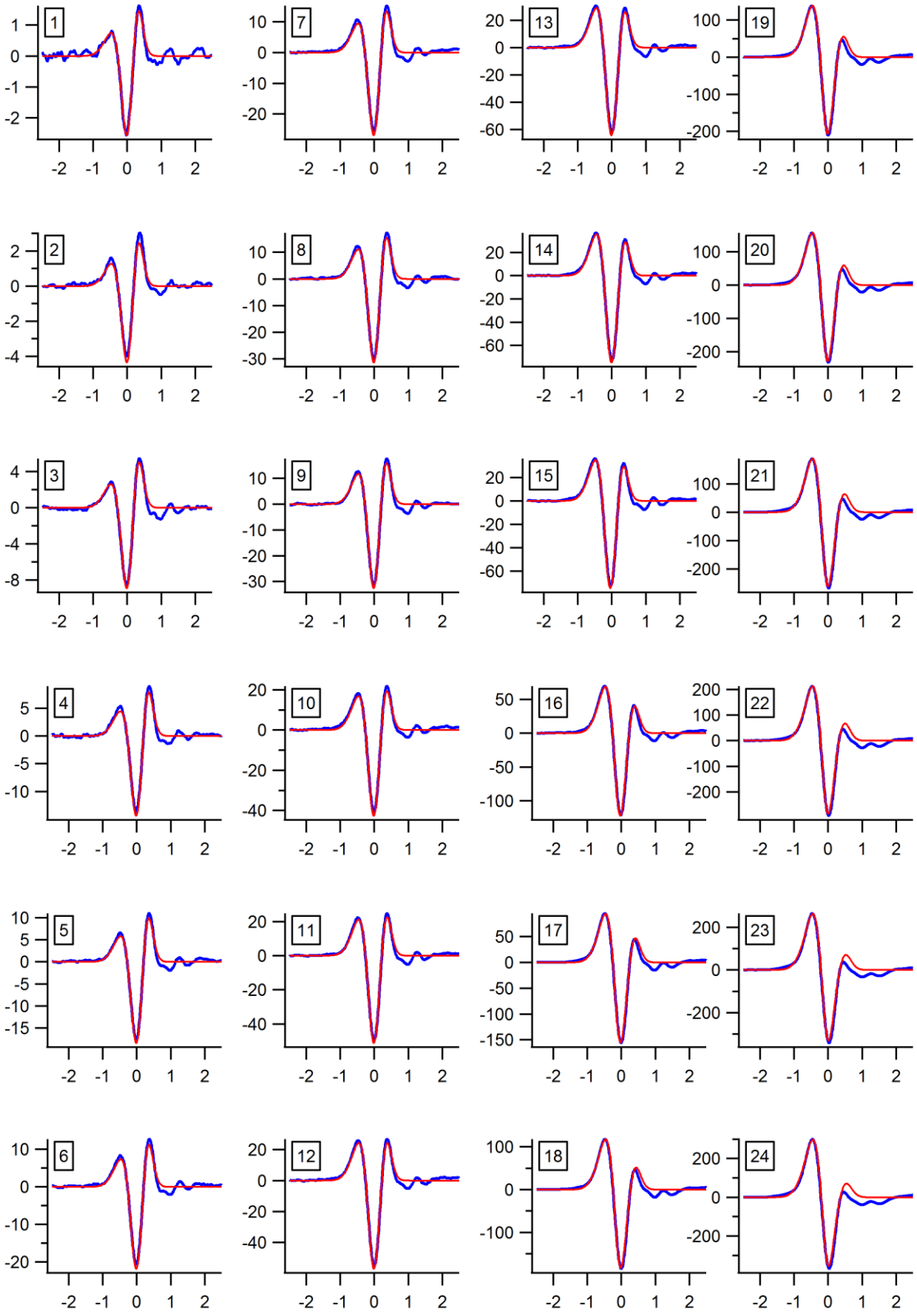

Figure S1. The 24 scans collected (thick blue lines) and the results of the nonlinear least squares fits (thin red lines).

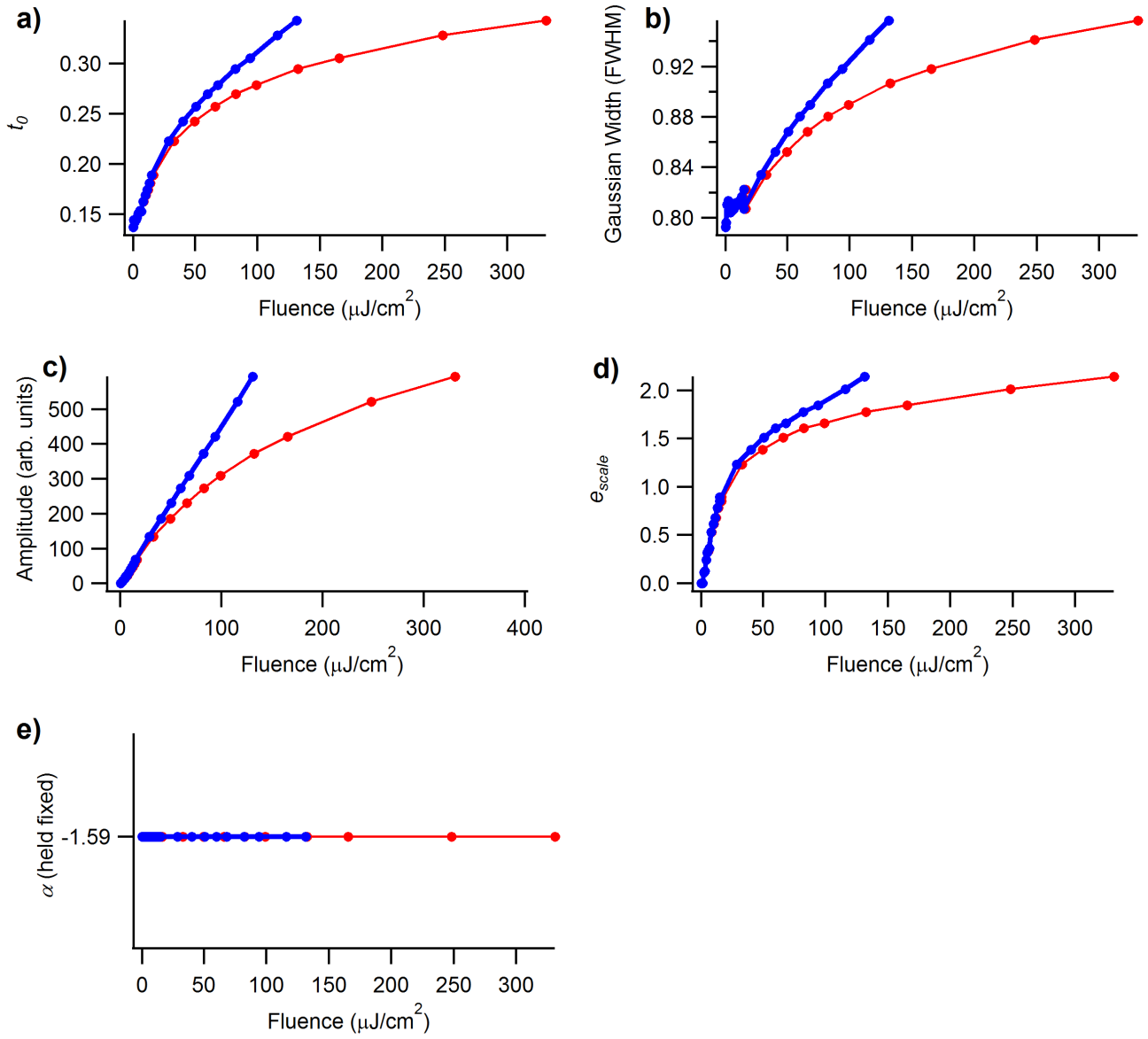

Figure S2. Fitting parameters as a function of fluence. The red circles connected by thin red lines are obtained when plotting each parameter as a function of fluence striking the sample. The thick blue lines are the same values for the parameters accounting for the loss of photons due to two-photon absorption; *i.e.*, the TPA-depleted fluence is used instead of the fluence striking the sample.

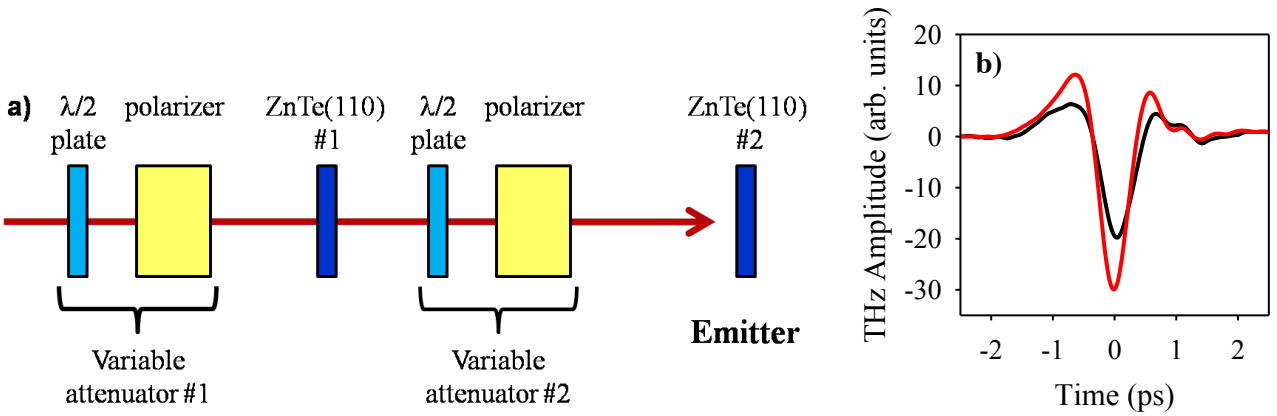

Figure S3. Part (a): Schematic of apparatus used to verify SPM as the source of THz pulse broadening and shifting as a function of excitation fluence. Part (b): Demonstration that THz emission is affected by high intensity light passing through ZnTe crystal #1. The fluence on ZnTe #1 was 69 μJ/cm^2 for the red waveform and 234 μJ/cm^2 for the black waveform. In both cases, the fluence at ZnTe #2 was 17 μJ/cm^2.

Table SI. Best fit parameters for waveforms shown in Figure 2a. Uncertainties in parentheses are 1σ. The entries in bold are those reported in Table I of the main text.

Fluence (μJ/cm^2)	**t_0 (ps)**	**FWHM (ps)**	**Amplitude**	**e_{scale}**	**α**
0.58	0.137(1.7)	0.792(5.7)	1.45(4.0)	1.00 x 10^{-5}*	-1.59*
0.89	**0.145(1.5)**	**0.796(5.2)**	**2.46(6.0)**	**1.00 x 10^{-5}***	**-1.59***
1.8	0.142(1.5)	0.810(4.9)	5.03(11)	1.00 x 10^{-5}*	-1.59*
2.7	0.144(1.3)	0.814(4.4)	8.66(17)	0.11(3.0)	-1.59*
3.6	0.147(1.2)	0.807(4.0)	11.2(2.1)	0.13(2.8)	-1.59*
4.4	0.151(1.3)	0.804(4.1)	14.2(2.6)	0.24(2.8)	-1.59*
5.3	0.152(1.4)	0.809(4.1)	18.3(3.3)	0.32(2.8)	-1.59*
6.2	0.154(1.3)	0.806(3.8)	21.6(3.6)	0.34(2.6)	-1.59*
7.1	0.153(1.2)	0.807(3.7)	22.7(3.6)	0.36(2.5)	-1.59*
8.9	0.163(1.2)	0.812(3.5)	32.8(4.7)	0.53(2.3)	-1.59*
11	0.169(1.3)	0.811(3.4)	41.3(5.6)	0.61(2.3)	-1.59*
12	0.174(1.3)	0.813(3.4)	47.6(6.3)	0.68(2.3)	-1.59*
14	0.181(1.3)	0.817(3.5)	56.6(7.3)	0.78(2.3)	-1.59*
17	**0.189(1.3)**	**0.822(3.3)**	**69.5(8.1)**	**0.89(2.1)**	**-1.59***
17	0.189(1.4)	0.807(3.5)	68.0(8.8)	0.85(2.3)	-1.59*
33	0.223(1.6)	0.834(3.7)	135(1.5)	1.23(2.3)	-1.59*
50	0.242(1.9)	0.852(4.1)	186(2.2)	1.38(2.5)	-1.59*
66	0.257(2.0)	0.868(4.3)	231(2.7)	1.51(2.6)	-1.59*
83	**0.270(2.2)**	**0.880(4.5)**	**274(3.2)**	**1.61(2.7)**	**-1.59***
99	0.279(2.3)	0.889(4.7)	310(3.6)	1.66(2.8)	-1.59*
132	0.295(2.6)	0.907(5.2)	372(4.6)	1.78(3.0)	-1.59*
166	0.306(2.8)	0.918(5.6)	421(5.3)	1.84(3.2)	-1.59*
248	0.328(3.4)	0.941(6.5)	522(7.0)	2.01(3.6)	-1.59*
331	**0.343(3.9)**	**0.957(7.4)**	**593(8.6)**	**2.14(4.1)**	**-1.59***

*These values were held fixed during the fit.